
DEEP KOOPMAN LEARNING OF NONLINEAR TIME-VARYING SYSTEMS

Wenjian Hao

School of Aeronautics and Astronautics Engineering
Purdue University, IN, USA
hao93@purdue.edu

Bowen Huang

Pacific Northwest National Laboratory
Richland, USA
bowen.h@pnnl.gov

Wei Pan

Department of Computer Science
University of Manchester, UK
wei.pan@tudelft.nl

Di Wu

Pacific Northwest National Laboratory
Richland, USA
di.wu@pnnl.gov

Shaoshuai Mou

School of Aeronautics and Astronautics Engineering
Purdue University, IN, USA
mous@purdue.edu

June 22, 2023

ABSTRACT

This paper presents a data-driven approach to approximate the dynamics of a nonlinear time-varying system (NTVS) by a linear time-varying system (LTVS), which is resulted from the Koopman operator and deep neural networks. Analysis of the approximation error between states of the NTVS and the resulting LTVS is presented. Simulations on a representative NTVS show that the proposed method achieves small approximation errors, even when the system changes rapidly. Furthermore, simulations in an example of quadcopters demonstrate the computational efficiency of the proposed approach.

1 Introduction

In recent years, data-driven methods have received a significant amount of research attention due to the increasing complexity of the autonomous systems in both dynamics [1–4] and mission objectives [5–7]. In the direction of learning system dynamics, the Koopman operator has recently been proven to be an effective method to approximate a nonlinear system by a linear time-varying system based on state-control pairs [2–4]. Along this direction, two popular methods dynamic mode decomposition (DMD) and extended dynamic mode decomposition (EDMD) are used to lift the state space to a higher-dimensional space, where the evolution is approximately linear [8]. However, choosing the proper observable functions for the lifting transformation is still an open question, and the potentially large lifted dimension may hinder real-time applications.

Recent work has proposed several methods for choosing proper observable functions of Koopman-based methods for time-invariant systems. Lusch et al. [9] proposed applying deep learning methods to discover the eigenfunctions of the approximated Koopman operator. Yeung et al. [10–13] introduced deep neural networks (DNN) as observable functions of the Koopman operator, which are tuned based on collected state-control pairs by minimizing a properly defined loss function. While some work, such as [14], has extended the DMD method to approximate nonlinear time-varying systems (NTVS) that change sufficiently slowly by linear time-varying systems (LTVS), this method is not directly applicable to approximate nonlinear systems with rapidly changing dynamics.

In this paper, we propose a deep Koopman learning method to approximate NTVS, which employs DNN as the observable function of the Koopman operator and adjusts both the DNN and the approximated dynamical system simultaneously. This is achieved by tuning the DNN parameters based on the latest state-control data pairs to track the unknown NTVS.

Compared to existing results in [14], the proposed method is able to approximate an NTVS which does not necessarily change slowly. Contributions of this paper are summarized as follows:

- We propose a deep Koopman representation formulation for the NTVS and provide a practical online algorithm for implementation.
- We investigate the error bound of the system state estimation of the proposed method.
- We perform a convergence analysis of the proposed method concerning the observable function of DNN.

This paper is organized as follows. In Section 2, we state the problem. Section 3 presents the main results. The numerical simulations are exhibited in Section 4. Finally, Section 5 concludes the paper.

Notations. Let $\|\cdot\|$ denote the Euclidean norm. For a matrix $A \in \mathbb{R}^{n \times m}$, $\|A\|_F$ denotes its Frobenius norm; A^T denotes its transpose; A^\dagger denotes its Moore-Penrose pseudoinverse. For positive integers n and m , \mathbf{I}_n denotes the $n \times n$ identity matrix; $\mathbf{0}_n \in \mathbb{R}^n$ denotes a vector with all value 0; $\mathbf{0}_{n \times m}$ denotes a $n \times m$ matrix with all value 0. $\text{sgn}(\cdot)$ denotes the sign function. $\lceil \cdot \rceil$ denotes the ceiling function, i.e., given real numbers y , integers k and the set of integers \mathbb{Z} , $\lceil y \rceil = \min\{k \in \mathbb{Z} \mid k \geq y\}$.

2 Problem Formulation

Consider an NTVS, the dynamics of which is unknown. Let $x_t \in \mathbb{R}^n$ and $u_t \in \mathbb{R}^m$ denote its state and control input at time t , respectively. $t \in [0, \infty)$ denotes the continuous-time index.

Suppose the states and control inputs can be obtained from unknown continuous NTVS at certain sampling time instances $t_k \in [0, \infty)$ with $k = 0, 1, 2, \dots$ the index of sampled data points. For notation brevity, one denotes $x_k := x_{t_k}$ and $u_k := u_{t_k}$ as the k -th observed system state and control input, respectively, in the remainder of this manuscript. Then one can partition the observed states-inputs pairs as the following series of data batches

$$\mathcal{B}_\tau = \{x_k, u_k : k \in \mathbb{K}_\tau\}, \quad \tau = 0, 1, 2, \dots, \quad (1)$$

where

$$\mathbb{K}_\tau = \{k_\tau, k_\tau + 1, k_\tau + 2, \dots, k_\tau + \beta_\tau\}$$

denotes the ordered labels set of sampling instances for the τ -th data batch \mathcal{B}_τ with β_τ positive integers such that

$$k_\tau = \sum_{i=0}^{\tau-1} \beta_i, \quad \tau \geq 1, \quad k_0 = 0.$$

It follows that

$$k_{\tau+1} = k_\tau + \beta_\tau, \quad \tau = 0, 1, 2, \dots,$$

which implies the last data in the τ -th data batch is the first data in $(\tau + 1)$ -th data batch. For notation simplicity, one defines $\mathcal{B}_\tau^x := \{x_k : k \in \mathbb{K}_\tau\}$, $\mathcal{B}_\tau^u := \{u_k : k \in \mathbb{K}_\tau\}$ in the rest of this manuscript. An illustration of the above indexes is shown in Fig. 1.

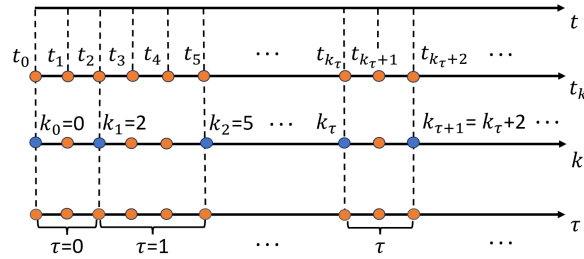


Figure 1: Time indexes, where blue color denotes k_τ .

This paper aims to develop an iterative method that approximates the dynamics of an unknown NTVS based on available data batches \mathcal{B}_τ by a linear time-varying discrete-time system. One way to achieve such a linear approximation is

by employing the Koopman operator as in [10–13]. Namely, based on the data batch \mathcal{B}_τ , one finds a nonlinear mapping $g(\cdot, \theta_\tau) : \mathbb{R}^n \rightarrow \mathbb{R}^r$ parameterized by $\theta_\tau \in \mathbb{R}^q$ ¹ and constant matrices $A_\tau \in \mathbb{R}^{r \times r}$, $B_\tau \in \mathbb{R}^{r \times m}$, $C_\tau \in \mathbb{R}^{n \times r}$ such that for $k \in \mathbb{K}_\tau$, $k < k_\tau + \beta_\tau$, the following holds approximately,

$$g(x_{k+1}, \theta_\tau) = A_\tau g(x_k, \theta_\tau) + B_\tau u_k, \quad (2)$$

$$x_{k+1} = C_\tau g(x_{k+1}, \theta_\tau). \quad (3)$$

Here, $g(\cdot, \theta_\tau)$, A_τ , B_τ , C_τ achieved from \mathcal{B}_τ are put together in the following $\mathcal{K}_{\mathcal{B}_\tau}$:

$$\mathcal{K}_{\mathcal{B}_\tau} := \{g(\cdot, \theta_\tau), A_\tau, B_\tau, C_\tau\}, \quad (4)$$

which is called a deep Koopman representation (DKR) in this manuscript.

Based on the DKR in (4), one could introduce $\hat{x}_k \in \mathbb{R}^n$ for $k \in \mathbb{K}_\tau$, $k < k_\tau + \beta_\tau$ as follows:

$$g(\hat{x}_{k+1}, \theta_\tau) = A_\tau g(\hat{x}_k, \theta_\tau) + B_\tau \hat{u}_k, \quad (5)$$

$$\hat{x}_{k+1} = C_\tau g(\hat{x}_{k+1}, \theta_\tau), \quad (6)$$

where

$$\hat{u}_k = u_k, \forall k \in \mathbb{K}_\tau, k < k_\tau + \beta_\tau, \quad \hat{x}_{k_\tau} = x_{k_\tau}. \quad (7)$$

This leads to the following linear system

$$\hat{x}_{k+1} = \hat{A}_\tau \hat{x}_k + \hat{B}_\tau \hat{u}_k, \quad k \in \mathbb{K}_\tau, k < k_\tau + \beta_\tau, \quad (8)$$

with $\hat{A}_\tau = C_\tau A_\tau C_\tau^\dagger$, $\hat{B}_\tau = C_\tau B_\tau$ and initial conditions in (7). The system (8) can be viewed as a linear approximation to the NTVS based on the data batch \mathcal{B}_τ . Note that when for any data batch \mathcal{B}_τ , one has A_τ, B_τ, C_τ remain constant for $k \in \mathbb{K}_\tau$. It follows that (8) is a linear time-invariant system for $k \in \mathbb{K}_\tau$.

To sum up, the **problem of interest** is to develop an iterative update rule to achieve a DKR in (4) based on data batch \mathcal{B}_τ in (1) such that the linear system (8) is a nice approximation of the unknown NTVS, i.e. \hat{x}_k (8) is close to x_k observed in \mathcal{B}_τ from the unknown NTVS in the sense that for any given accuracy $\varepsilon \geq 0$, $\hat{u}_k = u_k$ and $\hat{x}_{k_\tau} = x_{k_\tau}$, the estimation error $\|\hat{x}_k - x_k\| \leq \varepsilon$.

3 Main Results

This section proposes an algorithm to achieve a deep Koopman representation (DKR) that can approximate an unknown NTVS. We then investigate the estimation error between the state obtained from this DKR, as given in (8), and the observed state of the unknown NTVS.

3.1 Key Idea

Motivated by deep Koopman operator-based methods developed in [10–13], an optimal θ_τ for the deep Koopman representation (DKR), denoted by θ_τ^* , can be obtained by solving the following optimization problem based on the data batch \mathcal{B}_τ :

$$\theta_\tau^* = \arg \min_{\theta_\tau \in \mathbb{R}^q} \{w \mathbf{L}_1(A_\tau, B_\tau, \theta_\tau) + (1 - w) \mathbf{L}_2(C_\tau, \theta_\tau)\}, \quad (9)$$

where

$$\mathbf{L}_1(A_\tau, B_\tau, \theta_\tau) = \frac{1}{\beta_\tau} \sum_{k=k_\tau}^{k_\tau + \beta_\tau - 1} \|g(x_{k+1}, \theta_\tau) - (A_\tau g(x_k, \theta_\tau) + B_\tau u_k)\|^2 \quad (10)$$

and

$$\mathbf{L}_2(C_\tau, \theta_\tau) = \frac{1}{\beta_\tau} \sum_{k=k_\tau}^{k_\tau + \beta_\tau - 1} \|x_k - C_\tau g(x_k, \theta_\tau)\|^2. \quad (11)$$

The objectives of (10) and (11) are to approximate (2) and (3), respectively. Here, $0 < w < 1$ is a constant that combines the objective of minimizing \mathbf{L}_1 and \mathbf{L}_2 . In simple terms, \mathbf{L}_1 and \mathbf{L}_2 measure the simulation errors in the lifted and original coordinates, respectively.

¹Here, $g(\cdot, \theta_\tau)$ is usually represented by a DNN with a known structure g and an adjustable parameter $\theta_\tau \in \mathbb{R}^q$.

To solve (9), one needs to rewrite the available data batch and objective functions \mathbf{L}_1 and \mathbf{L}_2 in compact forms. Toward this end, the following notation is introduced:

$$\begin{aligned}\mathbf{X}_\tau &= [x_{k_\tau}, x_{k_\tau+1}, \dots, x_{k_\tau+\beta_\tau-1}] \in \mathbb{R}^{n \times \beta_\tau}, \\ \bar{\mathbf{X}}_\tau &= [x_{k_\tau+1}, x_{k_\tau+2}, \dots, x_{k_\tau+\beta_\tau}] \in \mathbb{R}^{n \times \beta_\tau}, \\ \mathbf{U}_\tau &= [u_{k_\tau}, u_{k_\tau+1}, \dots, u_{k_\tau+\beta_\tau-1}] \in \mathbb{R}^{m \times \beta_\tau}.\end{aligned}$$

Then \mathbf{L}_1 in (10) and \mathbf{L}_2 in (11) can be rewritten as

$$\mathbf{L}_1 = \frac{1}{\beta_\tau} \|\bar{\mathbf{G}}_\tau - (A_\tau \mathbf{G}_\tau + B_\tau \mathbf{U}_\tau)\|_F^2 \quad (12)$$

and

$$\mathbf{L}_2 = \frac{1}{\beta_\tau} \|\mathbf{X}_\tau - C_\tau \mathbf{G}_\tau\|_F^2, \quad (13)$$

where

$$\begin{aligned}\mathbf{G}_\tau &= [g(x_{k_\tau}, \theta_\tau), \dots, g(x_{k_\tau+\beta_\tau-1}, \theta_\tau)] \in \mathbb{R}^{r \times \beta_\tau}, \\ \bar{\mathbf{G}}_\tau &= [g(x_{k_\tau+1}, \theta_\tau), \dots, g(x_{k_\tau+\beta_\tau}, \theta_\tau)] \in \mathbb{R}^{r \times \beta_\tau}.\end{aligned} \quad (14)$$

By minimizing \mathbf{L}_1 with respect to A_τ, B_τ in (12) and minimizing \mathbf{L}_2 regarding C_τ in (13), A_τ, B_τ, C_τ can be determined by θ_τ as follows:

$$[A_\tau^\theta, B_\tau^\theta] = \bar{\mathbf{G}}_\tau \begin{bmatrix} \mathbf{G}_\tau \\ \mathbf{U}_\tau \end{bmatrix}^\dagger, \quad (15)$$

$$C_\tau^\theta = \mathbf{X}_\tau \mathbf{G}_\tau^\dagger. \quad (16)$$

Replacing A_τ and B_τ in (10) by (15) and C_τ in (11) by (16), the objective function in (9) can be reformulated as

$$\mathbf{L}(\theta_\tau) = \frac{1}{\beta_\tau} \sum_{k=k_\tau}^{k_\tau+\beta_\tau-1} \left\| \begin{bmatrix} g(x_{k+1}, \theta_\tau) \\ x_k \end{bmatrix} - K_\tau^\theta \begin{bmatrix} g(x_k, \theta_\tau) \\ u_k \end{bmatrix} \right\|^2, \quad (17)$$

with

$$K_\tau^\theta = \begin{bmatrix} A_\tau^\theta & B_\tau^\theta \\ C_\tau^\theta & \mathbf{0}_{n \times m} \end{bmatrix}.$$

Applying the existing deep Koopman operator methods developed in [10–13] to achieve the DKR by solving (9) based on each \mathcal{B}_τ available has two shortcomings. First, computing the pseudo-inverse in (15) and (16) repeatedly while solving (9) becomes computationally expensive as τ increases. Second, θ_τ must be initialized for each \mathcal{B}_τ , which can be challenging in time-varying systems applications. To overcome these two limitations, one can apply the deep Koopman operator method to approximate the unknown NTVS efficiently, and we propose the following method.

3.2 Algorithm

Before proceeding, we need the following assumption.

Assumption 1 The matrix $\mathbf{G}_\tau \in \mathbb{R}^{r \times \beta_\tau}$ in (14) and $\begin{bmatrix} \mathbf{G}_\tau \\ \mathbf{U}_\tau \end{bmatrix} \in \mathbb{R}^{(r+m) \times \beta_\tau}$ are of full row rank.

Remark 1 Assumption 1 is to ensure the matrices $\mathbf{G}_\tau \in \mathbb{R}^{r \times \beta_\tau}$ and $\begin{bmatrix} \mathbf{G}_\tau \\ \mathbf{U}_\tau \end{bmatrix} \in \mathbb{R}^{(r+m) \times \beta_\tau}$ invertible and it naturally requires $\beta_\tau \geq r + m$.

Lemma 1 Given $\mathcal{K}_{\mathcal{B}_\tau}$ in (4), if Assumption 1 holds, then the matrices $A_{\tau+1}^\theta, B_{\tau+1}^\theta, C_{\tau+1}^\theta$ can be achieved by

$$[A_{\tau+1}^\theta, B_{\tau+1}^\theta] = (\bar{\mathbf{G}}_{\tau+1} - [A_\tau^\theta, B_\tau^\theta] \chi_{\tau+1}) \lambda_\tau \chi_{\tau+1}^T (\chi_\tau \chi_\tau^T)^{-1} + [A_\tau^\theta, B_\tau^\theta], \quad (18)$$

$$C_{\tau+1}^\theta = (\mathbf{X}_{\tau+1} - C_\tau^\theta \mathbf{G}_{\tau+1}) \bar{\lambda}_\tau \mathbf{G}_{\tau+1}^T (\mathbf{G}_\tau \mathbf{G}_\tau^T)^{-1} + C_\tau^\theta, \quad (19)$$

where $\chi_\tau = \begin{bmatrix} \mathbf{G}_\tau \\ \mathbf{U}_\tau \end{bmatrix} \in \mathbb{R}^{(r+m) \times \beta_\tau}$, $\lambda_\tau = (\mathbf{I}_{\beta_{\tau+1}} + \chi_{\tau+1}^T (\chi_\tau \chi_\tau^T)^{-1} \chi_{\tau+1})^{-1} \in \mathbb{R}^{\beta_{\tau+1} \times \beta_{\tau+1}}$, $\bar{\lambda}_\tau = (\mathbf{I}_{\beta_{\tau+1}} + \mathbf{G}_{\tau+1}^T (\mathbf{G}_\tau \mathbf{G}_\tau^T)^{-1} \mathbf{G}_{\tau+1})^{-1} \in \mathbb{R}^{\beta_{\tau+1} \times \beta_{\tau+1}}$ with $\mathbf{G}_{\tau+1} \in \mathbb{R}^{r \times \beta_{\tau+1}}$, $\bar{\mathbf{G}}_{\tau+1} \in \mathbb{R}^{r \times \beta_{\tau+1}}$ defined in (14).

The proof of Lemma 1 will be given in [15].

To initialize the algorithm, one first needs to build the DNN $g(\cdot, \theta_\tau) : \mathbb{R}^n \rightarrow \mathbb{R}^r$ with non-zero $\theta_\tau \in \mathbb{R}^q$. Then the matrices $A_\tau^\theta \in \mathbb{R}^{r \times r}$, $B_\tau^\theta \in \mathbb{R}^{r \times m}$ and $C_\tau^\theta \in \mathbb{R}^{n \times r}$ can be found by solving (15) and (16), respectively, based on \mathcal{B}_τ . When the data batch $\mathcal{B}_{\tau+1}$ becomes available, one can directly update the $\mathbf{G}_{\tau+1}$ and $\bar{\mathbf{G}}_{\tau+1}$ by following (14), which leads to the $\chi_{\tau+1}$, λ_τ and $\bar{\lambda}_\tau$ in Lemma 1. Thus one can update A_τ^θ , B_τ^θ and C_τ^θ efficiently by computing (18)-(19) instead of solving (15)-(16) repeatedly as a consequence of applying Lemma 1. Finally, an optimal $\theta_{\tau+1}^*$ is obtained by solving (9) with $A_{\tau+1}^\theta$, $B_{\tau+1}^\theta$ subject to (18) and $C_{\tau+1}^\theta$ satisfying (19) based on $\mathcal{B}_{\tau+1}$.

To sum up, we have the following algorithm, which is referred to as deep Koopman learning for time-varying systems (DKTV) in the remainder of this manuscript and its pseudocode is provided in [15].

1. Initialization: Build $g(\cdot, \theta_\tau) : \mathbb{R}^n \rightarrow \mathbb{R}^r$ with $\theta_\tau \in \mathbb{R}^q$, $\theta_\tau \neq \mathbf{0}_q$; initialize A_τ^θ , B_τ^θ and C_τ^θ by solving (15) and (16), respectively, based on \mathcal{B}_τ .
2. When $\mathcal{B}_{\tau+1}$ becomes available, update A_τ^θ , B_τ^θ and C_τ^θ according to (18) and (19), respectively.
3. Solve (9) to find $\theta_{\tau+1}^*$, $A_{\tau+1}^{\theta^*}$, $B_{\tau+1}^{\theta^*}$ and $C_{\tau+1}^{\theta^*}$.
4. Repeat steps 2-3 as the unknown NTVS evolves.

3.3 Analysis of the Approximation Error

With a slight abuse of notation, suppose one observes the latest \mathcal{B}_τ with $\{x_{k-1}, u_{k-1}\}$ its latest data point (i.e., $x_{k-1} := x_{k_\tau + \beta_\tau}$, $u_{k-1} := u_{k_\tau + \beta_\tau}$), in this subsection, we investigate the estimation errors induced by the proposed algorithm described as:

$$e_k = \hat{x}_k - x_k, \quad (20)$$

where $\hat{x}_k \in \mathbb{R}^n$ denotes the estimated state achieved by the proposed method and $x_k \in \mathbb{R}^n$ denotes the state of the unknown NTVS evolving from $x_{k-1} \in \mathbb{R}^n$ and $u_{k-1} \in \mathbb{R}^m$. Here, to analyze the (20) with respect to $\theta_\tau \in \mathbb{R}^q$, one rewrites (5)-(6) as:

$$\hat{x}_k = C_\tau(A_\tau g(\hat{x}_{k-1}, \theta_\tau) + B_\tau \hat{u}_{k-1}), \quad (21)$$

with condition (7) hold.

Before we present the results, the following concepts about operators are introduced.

3.3.1 Preliminaries

Definition 1 (Koopman operator with control) Consider the Hilbert space \mathcal{F} and discrete-time nonlinear time-varying system $x_{k+1} = f(x_k, u_k, k)$ starting from time k_0 , where $k \in \mathbb{Z}$ denotes its time index; $x_k \in \mathcal{M}$ and $u_k \in \mathcal{U}$ denote the system state and control input at time k , respectively; $\mathcal{M} \subseteq \mathbb{R}^n$ and $\mathcal{U} \subseteq \mathbb{R}^m$ denote the state space and control input space, respectively. Then the dynamics of the states of the augmented control system z_k, z_{k+1} is described by

$$z_{k+1} = F(z_k, k) := \begin{bmatrix} f(x_k, \mathbf{u}(0), k) \\ \mathcal{S}\mathbf{u} \end{bmatrix},$$

where $z_k = \begin{bmatrix} x_k \\ \mathbf{u} \end{bmatrix}$ denotes the augmented control system states; $\mathcal{S}\mathbf{u}$ denotes the left shifting of the control sequence \mathbf{u} , i.e., $(\mathcal{S}\mathbf{u})(i) = \mathbf{u}(i+1)$ and $\mathbf{u}(i)$ denotes the i th element of the control sequence \mathbf{u} .

We then extend the definition of the Koopman operator from [16] to discrete-time NTVS. Let operator $\mathcal{K}^{(k_0, k)} : \mathcal{F} \rightarrow \mathcal{F}$ act on functions of state space $\phi(\cdot) \in \mathcal{F}$ with $\phi(\cdot) : \mathcal{M} \times \mathcal{U} \rightarrow \mathbb{C}$ and defined with two parameters (k_0, k) as

$$\mathcal{K}^{(k_0, k)}[\phi(z_k)] = \phi(F(z_k, k)).$$

Definition 2 (L_2 -projection [17]) For brevity, we recall the definitions of \mathcal{F} , \mathcal{M} , and $\phi(\cdot)$ from Definition 1. Let $\nu \in \mathbb{R}$ be the positive measure on \mathcal{M} and assume that $\mathcal{F} = L_2(\nu)$. Given a set of linearly independent $\phi_i \in \mathcal{F}$ with $i = 1, 2, \dots, r$, and define

$$\begin{aligned} \mathcal{F}_r &:= \text{span}\{\phi_1, \phi_2, \dots, \phi_r\}, \\ \Phi_r &= [\phi_1, \phi_2, \dots, \phi_r]^T. \end{aligned}$$

Then for all nonzero $c \in \mathbb{R}^r$, the $L_2(\nu)$ projection of a function $\psi \in L_2(\nu)$ on \mathcal{F}_r is defined as

$$P_r^\nu \psi = \arg \min_{f \in \mathcal{F}_r} \|f - \psi\|_{L_2(\nu)} = \arg \min_{f \in \mathcal{F}_r} \int_{\mathcal{M}} |f - \psi|^2 d\nu = \arg \min_{c \in \mathbb{R}^r} \int_{\mathcal{M}} |c^\top \Phi_r - \psi|^2 d\nu.$$

Definition 3 (Bounded operator) Given a Hilbert space \mathcal{F} , an operator $\mathcal{O} : \mathcal{F} \rightarrow \mathcal{F}$ is bounded on \mathcal{F} if

$$\|\mathcal{O}\| := \sup_{f \in \mathcal{F}, \|f\|=1} \|\mathcal{O}f\| < \infty.$$

$\|\mathcal{O}\|$ is referred as the operator norm of \mathcal{O} in the remainder of this manuscript.

Definition 4 (Strong Convergence of operator) A sequence of bounded operators $\mathcal{O}_i : \mathcal{F} \rightarrow \mathcal{F}$ defined on a Hilbert space \mathcal{F} converges strongly (or in the strong operator topology) to an operator $\mathcal{O} : \mathcal{F} \rightarrow \mathcal{F}$ if

$$\lim_{i \rightarrow \infty} \|\mathcal{O}_i f - \mathcal{O}f\| = 0$$

for all $f \in \mathcal{F}$.

3.3.2 Analysis

We make the following assumptions to show that the error e_k in (20) is bounded.

Assumption 2 For any \mathcal{B}_τ in (1), let $\{x_i, u_i\}$ denote its i th data point observed at time t_i . The observation interval $\Delta t = t_{i+1} - t_i$ is sufficiently small such that for some $\mu_x \geq 0, \mu_u \geq 0, \|x_{i+1} - x_i\| \leq \mu_x < \infty$ and $\|u_{i+1} - u_i\| \leq \mu_u < \infty$.

Assumption 3 The deep neural network observable function $g(\cdot, \theta_\tau)$ is Lipschitz continuous on the system state space with Lipschitz constant μ_g .

Consider a DNN observable function $g(\cdot, \theta_\tau) : \mathbb{R}^n \rightarrow \mathbb{R}^r$, let $\bar{\psi}^h = [\bar{\psi}_1^h, \bar{\psi}_2^h, \dots, \bar{\psi}_{n_h}^h]^T \in \mathbb{R}^{n_h}$ be its last hidden layer and $\bar{\psi}^o = [\bar{\psi}_1^o, \bar{\psi}_2^o, \dots, \bar{\psi}_r^o]^T \in \mathbb{R}^r$ denotes its output layer, where $\bar{\psi}_i^h : \mathbb{R} \rightarrow \mathbb{R}$ and $\bar{\psi}_i^o : \mathbb{R} \rightarrow \mathbb{R}$ are generally nonlinear function chosen by user. Note that here n_h and r denote the number of nodes of $\bar{\psi}^h$ and $\bar{\psi}^o$, respectively.

Assumption 4 (1): Given a Hilbert space \mathcal{F} , the Koopman operator \mathcal{K} is bounded and continuous on \mathcal{F} ; (2): $\bar{\psi}^h$ are selected from the orthonormal basis of \mathcal{F} , i.e., $[\bar{\psi}_1^h, \bar{\psi}_2^h, \dots, \bar{\psi}_\infty^h]^T$ is an orthonormal basis of \mathcal{F} .

Remark 2 Since the DNN observable function $g(x, \theta_\tau)$ is with known structure, one can make Assumption 4 hold by choosing proper activation functions for DNN's different layers. We refer to [18] for more details about candidate functions like radial basis functions.

Lemma 2 Let $\mu \in \mathbb{R}$ be the empirical measurements associated with the observed states $x_k \in \mathbb{R}^n$. If Assumption 4 holds, then the operator $P_{n_h}^\mu$ converges strongly to the identity operator I as n_h goes to infinity.

Proof of Lemma 2 is referred to in [15].

Lemma 3 Let $P := \begin{bmatrix} P_{n_h}^{\mu_1} & \mathbf{0}_{n_h \times m} \\ \mathbf{0}_{m \times n_h} & P_m^{\mu_2} \end{bmatrix}$ with $\mu_1 \in \mathbb{R}, \mu_2 \in \mathbb{R}$ the empirical measurements associated to the observed system state $x_k \in \mathbb{R}^n$ and control input $u_k \in \mathbb{R}^m$, respectively. If Assumption 4 holds, then the approximated sequence of operators $\mathcal{K}_D P = P \mathcal{K} P$ converges to Koopman operator \mathcal{K} strongly as n_h goes to infinity.

Proof of Lemma 3 is given in [15].

Remark 3 Lemma 3 shows the convergence condition of the existing DKO method regarding the DNN observable function $g(\cdot, \theta_\tau)$ ($n_h \rightarrow \infty$). It replaces the convergence condition of the EDMD method [17] ($r \rightarrow \infty$). This conclusion is used in the present work to reduce $\beta_\tau \geq r + m$ so that one can track the unknown NTVS based on \mathcal{B}_τ with small batch size.

Theorem 1 Let $g(x, \theta_\tau)$ be a DNN with its last hidden layer containing n_h nodes. If Assumptions 1-4 hold, then the estimation error e_k in (20) is bounded by

$$\lim_{n_h \rightarrow \infty} \sup \|e_k\| = (\|C_\tau A_\tau\| \mu_g + 1) \mu_x + \|C_\tau B_\tau\| \mu_u + \max_{\bar{x} \in \mathcal{B}_\tau^x} \|\bar{x} - C_\tau g(\bar{x}, \theta_\tau)\|.$$

The proof of Theorem 1 is given in [15].

Remark 4 *Theorem 1* says that with certain assumptions hold, as $n_h \rightarrow \infty$, the estimation error of the proposed method depends on the minimization performance of (13) and μ_x, μ_u defined in Assumption 2. One way to further reduce the estimation error is to decrease the sampling interval.

Since one cannot construct a DNN with infinite parameters in practice, we introduce the following corollary based on Theorem 1, for which we need to make the following assumption.

Assumption 5 For any $A_\tau \in \mathbb{R}^{r \times r}$, $\|A_\tau\| < 1$.

Remark 5 According to Lemma 1, the DNN observable function determines $\|A_\tau\|$. To make Assumption 5 hold, one can add an extra loss function to impose the maximum value of $\|A_\tau\|$ in (9).

Corollary 1 Recall e_k in (20). If Assumptions 1-3 and 5 hold, then the upper bound of $\|e_k\|$ is determined by the minimization performance of (17) and μ_x, μ_u as k goes to infinity.

The proof of Corollary 1 is given in [15].

4 Numerical Simulations

In this section, we test the proposed algorithm in two examples, one is a simple nonlinear time-varying system (NTVS), and the other one is a quadcopter. In both examples, the system state input data is observed with a fixed time interval of 0.1s, and $\beta_\tau \equiv \beta$, where $\beta \geq r + m$ is an arbitrary positive integer, and $\tau = \lceil \frac{k - \beta_0}{\beta} \rceil$, where $k \in \mathbb{K}_\tau$.

4.1 A Simple NTVS

Consider the following dynamical system:

$$\dot{x}_t = M_t \cos(x_t), \quad (22)$$

where $x_t \in \mathbb{R}^2$ and M_t is a time-varying matrix given by

$$M_t = \begin{bmatrix} 0 & (1 + \gamma t) \\ -(1 + \gamma t) & 0 \end{bmatrix}, \quad (23)$$

where γ is a constant determining how fast the dynamics change. For more details of the dynamics, see [14].

Experiment Setup. The DNN observable function $(g(\cdot, \theta) : \mathbb{R}^2 \rightarrow \mathbb{R}^6)$ is built with a hidden layer $ReLU()$ that contains 32 nodes and an output layer $Relu()$ consisting of 6 nodes. The DNN training process is implemented by choosing optimizer *Adam* [19] with *learning rate* = $1e-3$ and *weight decay rate* = $1e-4$. Then \mathcal{B}_τ is observed with $\beta = 10$ starting from $x_0 = [1, 0]^T$.

Remark 6 The activation function $ReLU()$ is selected for this example because by appropriately selecting x_0 and γ , one can ensure that $x_t \geq 0$. This choice results in $ReLU(x) = x$ which belongs to the category of linear radial basis functions [20].

Results Analysis. We test the proposed method in the NTVS in (22) for both slow and fast-changing scenarios setting $\gamma = 0.8$ and $\gamma = 6$, respectively. The trajectories estimated by time-varying DMD(TVDMD) and the proposed method are shown in Figs. 2, and the estimation errors of both methods are exhibited in Fig. 3. Here, we let $x_k \in \mathbb{R}^2$ denote the true system states observed from the unknown NTVS. Let $\tilde{x}_k \in \mathbb{R}^2$ denote the estimated states generated by the TVDMD method from [14]. Let $\hat{x}_k \in \mathbb{R}^2$ be the estimated states from the proposed method (DKTV), as given in (21). Consequently, $\tilde{e}_k = \|\tilde{x}_k - x_k\|$ and $e_k = \|\hat{x}_k - x_k\|$ denote the estimation errors induced by the TVDMD and DKTV methods, respectively. It can be observed that when the NTVS varies slowly, both methods can capture the dynamics of the NTVS with reasonable accuracy. In situations where the NTVS varies rapidly, the estimation errors of the TVDMD method increase correspondingly. On the contrary, the proposed method can achieve consistent performance, benefiting from its DNN observable function.

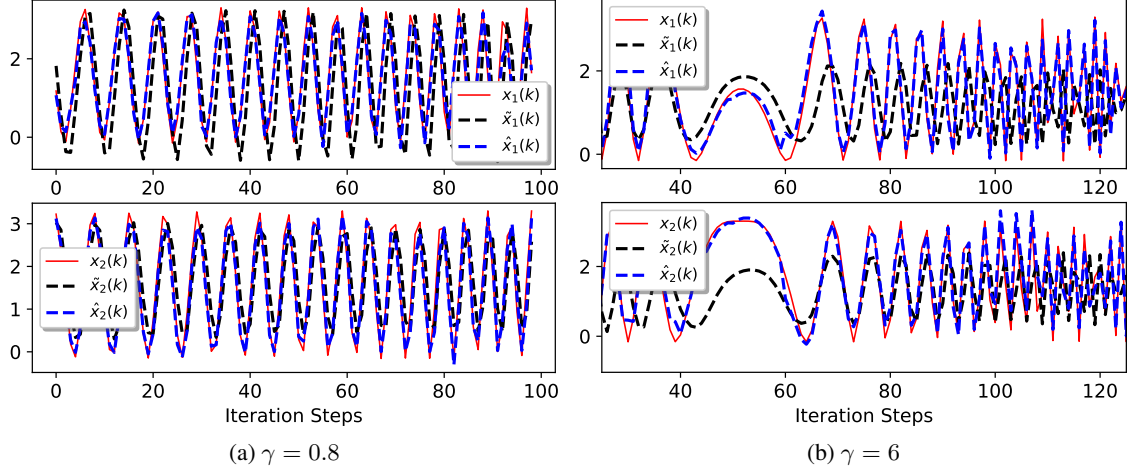


Figure 2: System states trajectories: TVDMD (black) vs. DKTV (blue).

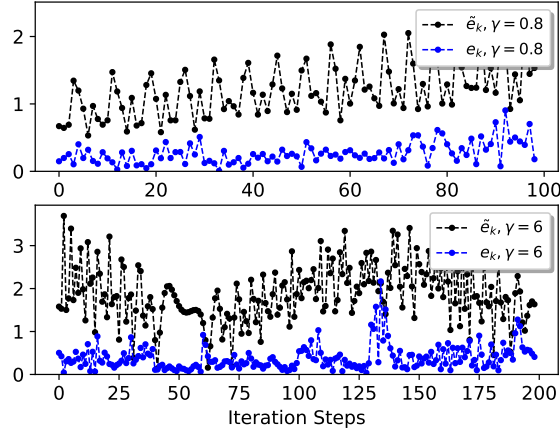


Figure 3: System states estimation errors: TVDMD (black) vs. DKTV (blue).

4.2 System States Prediction for Single Quadcopter

In this example, we implement the proposed algorithm to predict the system states of a quadcopter with a time-varying disturbance applied to its body. The dynamics of the quadcopter is described as

$$\begin{aligned} \begin{pmatrix} \dot{p}_n \\ \dot{p}_e \\ \dot{z} \end{pmatrix} &= \begin{pmatrix} c_\theta c_\psi & s_\phi s_\theta c_\psi - c_\phi s_\psi & c_\phi s_\theta c_\psi + s_\phi s_\psi \\ c_\theta s_\psi & s_\phi s_\theta s_\psi + c_\phi c_\psi & c_\phi s_\theta s_\psi - s_\phi c_\psi \\ s_\theta & -s_\phi c_\theta & -c_\phi c_\theta \end{pmatrix} \begin{pmatrix} \dot{x} \\ \dot{y} \\ \dot{z} \end{pmatrix}, \\ \begin{pmatrix} \dot{\phi} \\ \dot{\theta} \\ \dot{\psi} \end{pmatrix} &= \begin{pmatrix} 1 & s_\phi t_\theta & c_\phi t_\theta \\ 0 & c_\phi & -s_\phi \\ 0 & \frac{s_\phi}{c_\theta} & \frac{c_\phi}{s_\theta} \end{pmatrix} \begin{pmatrix} p \\ q \\ r \end{pmatrix}, \\ \begin{pmatrix} \ddot{x} \\ \ddot{y} \\ \ddot{z} \end{pmatrix} &= \begin{pmatrix} r\dot{y} - q\dot{z} \\ p\dot{z} - r\dot{x} \\ q\dot{x} - p\dot{y} \end{pmatrix} + \frac{1}{m} \begin{pmatrix} f_x \\ f_y \\ f_z \end{pmatrix} + w_t, \\ \begin{pmatrix} \dot{p} \\ \dot{q} \\ \dot{r} \end{pmatrix} &= \begin{pmatrix} \frac{J_y - J_z}{J_x} qr \\ \frac{J_z - J_x}{J_y} pr \\ \frac{J_x - J_y}{J_z} pq \end{pmatrix} + \begin{pmatrix} \frac{1}{J_x} \tau_\phi \\ \frac{1}{J_y} \tau_\theta \\ \frac{1}{J_z} \tau_\psi \end{pmatrix}, \end{aligned}$$

where s_θ , s_ϕ , s_ψ , c_θ , c_ϕ , c_ψ , and t_θ denote $\sin(\theta)$, $\sin(\phi)$, $\sin(\psi)$, $\cos(\theta)$, $\cos(\phi)$, $\cos(\psi)$, and $\tan(\theta)$, respectively. p_n , p_e , and z denote the inertial north position, the inertial east position, and the altitude, respectively. \dot{x} , \dot{y} , and \dot{z} denote the velocity along the x-axis, y-axis, and z-axis, respectively. ϕ , θ , and ψ denote the roll angle, pitch angle,

and yaw angle, respectively, and p , q , and r denote the roll rate, pitch rate, and yaw rate, respectively. f_x , f_y , and f_z denote the total force applied to the quadcopter along the x-axis, y-axis, and z-axis, respectively, and $w_t \in \mathbb{R}^3$ denotes the time-varying disturbance. τ_ϕ , τ_θ and τ_ψ denote the torque of roll, pitch, and yaw, respectively, while J_x , J_y , and J_z denote the inertia along the x-axis, y-axis, and z-axis, respectively. For further details on the dynamics of the quadcopter, see [21].

Experiment Setup. In order to compare the performance of the proposed algorithm with that of the single neural network method, we let $x_k \in \mathbb{R}^{12}$ denote the true state of the system, $\bar{x}_k \in \mathbb{R}^{12}$ and $\hat{x}_k \in \mathbb{R}^{12}$ denote the estimated states of the single DNN and the proposed method, respectively, and $\bar{e}_k = \|\bar{x}_k - x_k\|$ and $e_k = \|\hat{x}_k - x_k\|$ denote the estimation errors of the single DNN and DKTV methods, respectively. The data batch \mathcal{B}_τ is collected with $\beta = 30$ manually controlling the quadcopter from position (0, 0, 0) (meter) to (1, 2, 3) (meter) with the time-varying disturbance force $w_t \in \mathbb{R}^3$ applied on the quadcopter. w_t is generated from the standard normal distribution. For the DKTV method, the DNN observable function $g(\cdot, \theta) : \mathbb{R}^{12} \rightarrow \mathbb{R}^{16}$ is built with one hidden layer *Gaussian function* containing 64 nodes and one output layer *Relu()* consisting of 16 nodes. For the single DNN method, DNN $N(\cdot, \nu) : \mathbb{R}^{16} \rightarrow \mathbb{R}^{12}$ is built with the same structure as $g(\cdot, \theta)$. Then the DNN training process of both methods is implemented by choosing optimizer *Adam* [19] with *learning rate* = $1e-3$ and *weight decay rate* = $1e-4$. The optimal vector $\nu \in \mathbb{R}^p$ is found by

$$\nu^* = \arg \min_{\nu \in \mathbb{R}^p} L(\nu) = \arg \min_{\nu \in \mathbb{R}^p} \|N(x_k, u_k, \nu) - x_{k+1}\|, \quad (24)$$

which leads to $\bar{x}_{k+1} = N(x_k, u_k, \nu^*)$.

Results Analysis. We first show the DNN training process of both methods with $\tau = 1, \dots, 7$ in Fig. 4, where one epoch denotes one forward and one backward pass through the DNN and $L(\nu)$, $L(\theta)$ are defined in (24) and (17), respectively. As shown, DKTV needs fewer training epochs to converge and maintains a much lower loss value during the training process than the single DNN method, as expected due to its double minimization of (12)-(13). Then in

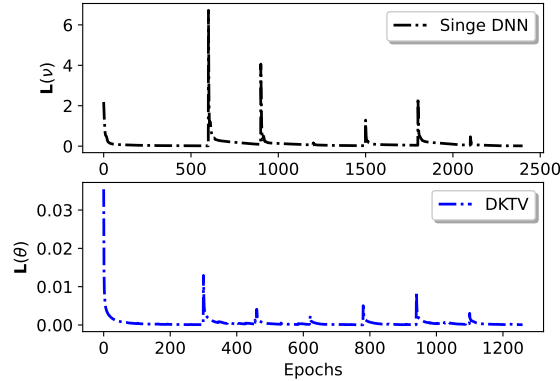


Figure 4: Training process: DNN (black) vs. DKTV (blue).

Fig. 5, we demonstrate the algorithm performance by showing the system states estimation errors of both methods. As is shown, the proposed algorithm can provide better prediction performance compared with the Single DNN method. Finally, in Fig. 6, Theorem 1 is validated by showing that the estimation errors of the proposed algorithm are reduced by increasing the number of nodes of its hidden layer.

4.3 Optimal Control based on the Proposed Deep Koopman Learning

In this subsection, we design the optimal controller based on the proposed method for a classic cartpole example from [22], where we make the coefficient of friction of cart on track ($\mu_c(t)$) time-varying during the simulation. And we choose the well-studied model predictive control (MPC) method to demonstrate the optimal control application based on the proposed algorithm, of which the optimization problem is formulated as

$$\begin{aligned} \min_{u_i, x_i} \quad & J(u_i, x_i) \\ \text{s.t.} \quad & u_i \in \mathcal{U}, x_i \in \mathcal{X}, i = k_\tau, \dots, k_\tau + \beta_\tau - 1, \\ & g(x_{i+1}, \theta_\tau) = A_\tau g(x_i, \theta_\tau) + B_\tau u_i, \\ & x_i = C_\tau g(x_i, \theta_\tau), \\ & x_{t+l} = x_l, \end{aligned} \quad (25)$$

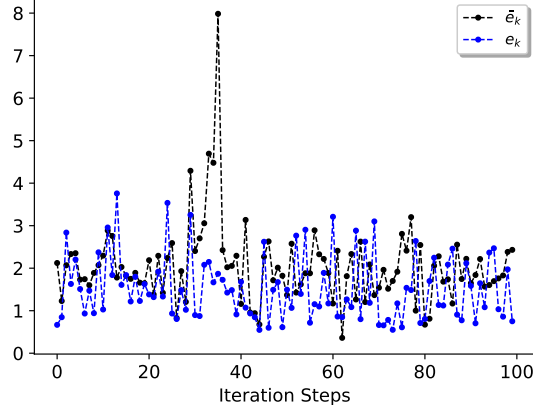


Figure 5: System states estimation error: DNN (black) vs. DKTV(blue).

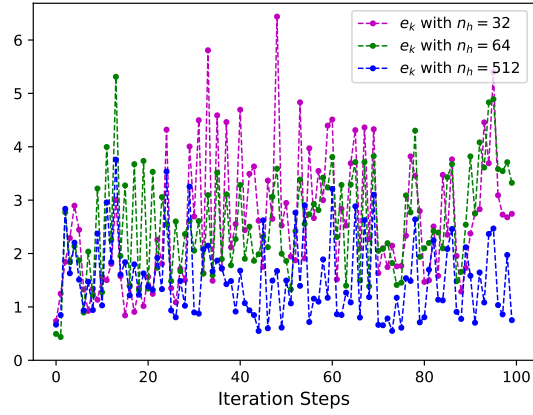


Figure 6: The estimation errors of DKTV with different DNN observable functions.

where $J(u_i, x_i)$ is defined by

$$J(u_i, x_i) = \sum_{i=k_\tau}^{k_\tau+l-1} (\bar{g}(x_i, \theta_\tau)^T \tilde{Q}_\tau \bar{g}(x_i, \theta_\tau) + u_i^T R u_i) + g(x_l, \theta_\tau)^T \tilde{Q}_l g(x_l, \theta_\tau),$$

and $l \leq \beta_\tau$ is the time horizon; i is the time-index along the defined time horizon; $x_i \in \mathbb{R}^n$ and $u_i \in \mathbb{R}^m$ are the system state and control input at time step i , respectively; $\bar{g}(x_i, \theta_\tau) = g(x_i, \theta_\tau) - g(x^*, \theta_\tau)$ with x^* denoting the goal state; x_l is the terminal state; \mathcal{X} denotes the state constraint and \mathcal{U} denotes the control input constraint; $\tilde{Q}_\tau = C_\tau^T Q C_\tau \in \mathbb{R}^{r \times r}$, $Q \in \mathbb{R}^{n \times n}$, $R \in \mathbb{R}^{m \times m}$ are positive definite matrices.

4.3.1 Time-varying Cartpole Balance

In this example, the physic governing equation of the cartpole is described as

$$\begin{aligned} \ddot{x}_t &= \frac{F_t + ml(\dot{\bar{\theta}}_t^2 \sin \bar{\theta}_t - \ddot{\bar{\theta}}_t \cos \bar{\theta}_t) - \mu_t^c \text{sgn}(\dot{x}_t)}{m_c + m} \\ \ddot{\bar{\theta}}_t &= \frac{\cos \theta_t [-F_t - ml\dot{\bar{\theta}}_t^2 \sin \theta_t + \mu_t^c \text{sgn}(\dot{x}_t)] / (m_c + m)}{l[\frac{4}{3} - (m \cos^2 \bar{\theta}_t) / (m_c + m)]} + \frac{g \sin \theta_t - \mu_p \dot{\bar{\theta}}_t / ml}{l[\frac{4}{3} - (m \cos^2 \bar{\theta}_t) / (m_c + m)]}, \end{aligned} \quad (26)$$

where $\mu_t^c = 0.3 \cos(t)$ with $\mu_0^c = 0.0005$ is the *time-varying* coefficient of friction of cart on track; x_t denotes the distance of the cartpole moves from the initial position; $\bar{\theta}_t$ denotes the angle from the up position; $\dot{x}_t, \dot{\bar{\theta}}_t$ denote the x-axis velocity and the angular velocity respectively; F_t denotes the continuous control input applied to the center of the mass of the cart at time step t ; $g = -9.8m/s^2$ is the gravity acceleration; $m_c = 1.0kg$, $m = 0.1kg$ are the mass of the cart and the pole, respectively; $l = 0.5m$ is the length of the pole; $\mu_p = 0.000002$ is the coefficient of the friction of the pole on cart.

For the simulation, we first build the DNN $(g(\cdot, \theta) : \mathbb{R}^4 \rightarrow \mathbb{R}^6)$ and set $\beta = 12$; then the \mathcal{B}_τ is generated by observing the dynamics in (26) with fixed time interval $t_{k_\tau+1} - t_{k_\tau} \equiv 0.1s$. The approximated dynamics is directly applied to design the MPC controller to keep the cartpole balanced at the up position with $\bar{\theta} = 0, \dot{\bar{\theta}} = 0$.

Results Analysis: Fig. 7 shows the trajectory of the time-varying cartpole under the MPC control based on the proposed method. From the result, the cartpole is able to keep the desired up position under the DKTV-based MPC control even though μ_k^c increases from 0.0005 to 14.288.

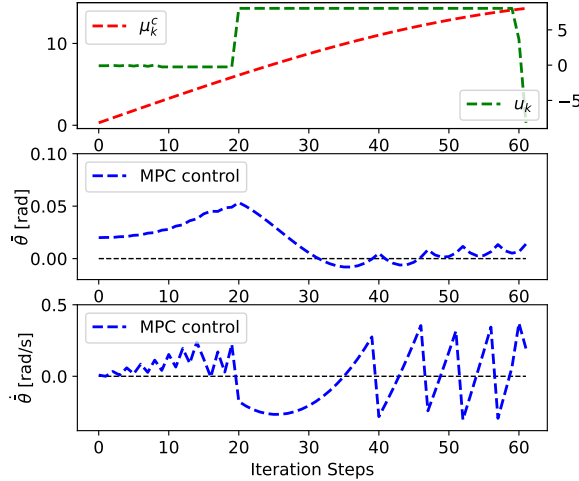


Figure 7: MPC based on the Approximated Dynamics

Remark 7 *In this subsection, we show the MPC design based on approximated linear dynamics from the proposed algorithm. Compared to the existing MPC method for the NTVS proposed in [23–25], the proposed method requires neither the priori knowledge of the system dynamics nor the distribution information of the system disturbance.*

5 Conclusions

This paper presents a data-driven approach to approximate the dynamics of a nonlinear time-varying system (NTVS) by a linear time-varying system (LTVS), which is resulted from the Koopman operator and deep neural networks. The proposed algorithm is able to approximate well an NTVS by iterative updating its linear approximation as validated by a simple NTVS system in two dimensions. Moreover, controllers developed based on linear approximation perform well in controlling a quadrotor with complex dynamics. Future work includes employing the proposed method to achieve adaptive autonomy in [26, 27] and to serve as robot’s dynamics estimation in human-robot teaming [28, 29].

References

- [1] Giorgos Mamakoukas, Maria L Castano, Xiaobo Tan, and Todd D Murphey. Derivative-based koopman operators for real-time control of robotic systems. *IEEE Transactions on Robotics*, 37(6):2173–2192, 2021.
- [2] Igor Mezić. On applications of the spectral theory of the koopman operator in dynamical systems and control theory. In *2015 54th IEEE Conference on Decision and Control (CDC)*, pages 7034–7041. IEEE, 2015.
- [3] Joshua L Proctor, Steven L Brunton, and J Nathan Kutz. Generalizing koopman theory to allow for inputs and control. *SIAM Journal on Applied Dynamical Systems*, 17(1):909–930, 2018.
- [4] Alexandre Mauroy and Jorge Goncalves. Linear identification of nonlinear systems: A lifting technique based on the koopman operator. In *2016 IEEE 55th Conference on Decision and Control (CDC)*, pages 6500–6505. IEEE, 2016.
- [5] W. Jin, D. Kulic, J. Lin, S. Mou, and S. Hirche. Inverse optimal control for multiple-phase cost functions. *IEEE Transactions on Robotics*, 35, 2019.
- [6] W. Jin and S. Mou. Distributed inverse optimal control. *Automatica*, (109658), 2021.

- [7] W. Jin, D. Kulic, S. Mou, and S. Hirche. Inverse optimal control from incomplete trajectory observations. *The International Journal of Robotics Research*.
- [8] Milan Korda and Igor Mezić. Linear predictors for nonlinear dynamical systems: Koopman operator meets model predictive control. *Automatica*, 93:149–160, 2018.
- [9] Bethany Lusch, Steven L Brunton, and J Nathan Kutz. Data-driven discovery of koopman eigenfunctions using deep learning. *Bulletin of the American Physical Society*, 2017.
- [10] Enoch Yeung, Soumya Kundu, and Nathan Hodas. Learning deep neural network representations for koopman operators of nonlinear dynamical systems. In *2019 American Control Conference (ACC)*, pages 4832–4839. IEEE, 2019.
- [11] Bethany Lusch, J Nathan Kutz, and Steven L Brunton. Deep learning for universal linear embeddings of nonlinear dynamics. *Nature communications*, 9(1):1–10, 2018.
- [12] Yiqiang Han, Wenjian Hao, and Umesh Vaidya. Deep learning of koopman representation for control. In *2020 59th IEEE Conference on Decision and Control (CDC)*, pages 1890–1895. IEEE, 2020.
- [13] Petar Bevanda, Max Beier, Sebastian Kerz, Armin Lederer, Stefan Sosnowski, and Sandra Hirche. Koopmanizingflows: Diffeomorphically learning stable koopman operators. *arXiv preprint arXiv:2112.04085*, 2021.
- [14] Hao Zhang, Clarence W Rowley, Eric A Deem, and Louis N Cattafesta. Online dynamic mode decomposition for time-varying systems. *SIAM Journal on Applied Dynamical Systems*, 18(3):1586–1609, 2019.
- [15] Wenjian Hao, Bowen Huang, Wei Pan, Di Wu, and Shaoshuai Mou. Deep koopman representation of nonlinear time varying systems. *arXiv preprint arXiv:2210.06272*, 2022.
- [16] Bowen Yi and Ian R Manchester. On the equivalence of contraction and koopman approaches for nonlinear stability and control. In *2021 60th IEEE Conference on Decision and Control (CDC)*, pages 4609–4614. IEEE, 2021.
- [17] Milan Korda and Igor Mezić. On convergence of extended dynamic mode decomposition to the koopman operator. *Journal of Nonlinear Science*, 28(2):687–710, 2018.
- [18] Matthew O Williams, Ioannis G Kevrekidis, and Clarence W Rowley. A data-driven approximation of the koopman operator: Extending dynamic mode decomposition. *Journal of Nonlinear Science*, 25(6):1307–1346, 2015.
- [19] Diederik P Kingma and Jimmy Ba. Adam: A method for stochastic optimization. *arXiv preprint arXiv:1412.6980*, 2014.
- [20] Isaac J Schoenberg. Metric spaces and positive definite functions. *Transactions of the American Mathematical Society*, 44(3):522–536, 1938.
- [21] Randal W Beard. Quadrotor dynamics and control. *Brigham Young University*, 19(3):46–56, 2008.
- [22] Andrew G Barto, Richard S Sutton, and Charles W Anderson. Neuronlike adaptive elements that can solve difficult learning control problems. *IEEE transactions on systems, man, and cybernetics*, (5):834–846, 1983.
- [23] Marko Tanaskovic, Lorenzo Fagiano, and Vojislav Gligorovski. Adaptive model predictive control for linear time varying mimo systems. *Automatica*, 105:237–245, 2019.
- [24] Pornchai Bumroongsri. Tube-based robust mpc for linear time-varying systems with bounded disturbances. *International Journal of Control, Automation and Systems*, 13(3):620–625, 2015.
- [25] Paolo Falcone, Manuela Tufo, Francesco Borrelli, Jahan Asgari, and H Eric Tseng. A linear time varying model predictive control approach to the integrated vehicle dynamics control problem in autonomous systems. In *2007 46th IEEE Conference on Decision and Control*, pages 2980–2985. IEEE, 2007.
- [26] W. Jin, Z. Wang, Z. Yang, and S. Mou. Pontryagin differentiable programming: An end-to-end learning and control framework. *Advances in Neural Information Processing Systems*, 3, 2020.
- [27] W. Jin, S. Mou, and G. J. Pappas. Safe pontryagin differentiable programming. *Advances in Neural Information Processing Systems (NeuIPS)*, 2021.
- [28] W. Jin, T. D. Murphey, Z. Lu, and S. Mou. Learning from human directional corrections. *IEEE Transactions on Robotics*, 2023.
- [29] W. Jin, T. D. Murphey, D. Kulic, N. Ezer, and S. Mou. Learning from human sparse demonstrations. *IEEE Transactions on Robotics*, 1, 2023.
- [30] Giorgos Mamakoukas, Ian Abraham, and Todd D Murphey. Learning data-driven stable koopman operators. *arXiv preprint arXiv:2005.04291*, 2020.

6 Appendix

Pseudocodes.

Algorithm 1 Deep Koopman Learning for Time-Varying Systems (DKTV)

Input: $\beta_0, \beta_1, \dots, \beta_\tau, \dots$
Output: $g(\cdot, \theta_\tau), A_\tau, B_\tau, C_\tau, \tau = 1, 2, \dots$
Initialization:

- Set $k = \beta_0, \tau = 0$, and empty matrices $\mathbf{X}, \bar{\mathbf{X}}, \mathbf{U}$ for temporary data storage.
- Initialize $g(\cdot, \theta_0)$ with random $\theta_0 \in \mathbb{R}^q$, and A_0, B_0, C_0 by (15)-(16) based on the observed \mathcal{B}_0 .

while 1 do

Insert $x_k \in \mathbb{R}^n, x_{k+1} \in \mathbb{R}^n, u_k \in \mathbb{R}^m$ as new columns into $\mathbf{X}, \bar{\mathbf{X}}, \mathbf{U}$, respectively.

 $k := k + 1.$
if $k = \sum_{i=0}^{\tau+1} \beta_i$ **then**
Set: $\tau := \tau + 1, \mathbf{X}_\tau := \mathbf{X}, \bar{\mathbf{X}}_\tau := \bar{\mathbf{X}}, \mathbf{U}_\tau := \mathbf{U}.$
Update: A_τ^θ and B_τ^θ are updated by (18), and C_τ^θ is updated by (19).

Build: Construct $\mathbf{L}(\theta_\tau)$ by (17) and solve

$$\theta_\tau^* = \arg \min_{\theta_\tau \in \mathbb{R}^q} \mathbf{L}(\theta_\tau).$$

Update: $A_\tau := A_\tau^{\theta^*}, B_\tau := B_\tau^{\theta^*}, C_\tau := C_\tau^{\theta^*}.$
Reset: $\mathbf{X} := \mathbf{X}_\tau[:, \beta_\tau], \bar{\mathbf{X}} := \bar{\mathbf{X}}_\tau[:, \beta_\tau],$
 $\mathbf{U} := \mathbf{U}_\tau[:, \beta_\tau].$
end

Proof of Lemma 1. Similar to the EDMD, we start by solving the least square problem with collected state-control pairs \mathcal{B}_τ in (1). Define

$$\mathbf{X}_\tau = [x_{k_\tau}, x_{k_\tau+1}, \dots, x_{k_\tau+\beta_\tau-1}] \in \mathbb{R}^{n \times \beta_\tau},$$

$$\bar{\mathbf{X}}_\tau = [x_{k_\tau+1}, x_{k_\tau+2}, \dots, x_{k_\tau+\beta_\tau}] \in \mathbb{R}^{n \times \beta_\tau},$$

$$\mathbf{U}_\tau = [u_{k_\tau}, u_{k_\tau+1}, \dots, u_{k_\tau+\beta_\tau-1}] \in \mathbb{R}^{m \times \beta_\tau}.$$

Given $g(\cdot, \theta_\tau) : \mathbb{R}^n \rightarrow \mathbb{R}^r$ with fixed vector $\theta_\tau \in \mathbb{R}^q$, matrices $A_\tau \in \mathbb{R}^{r \times r}, B_\tau \in \mathbb{R}^{r \times m}$ are obtained by solving

$$\min_{A_\tau \in \mathbb{R}^{r \times r}, B_\tau \in \mathbb{R}^{r \times m}} \|\bar{\mathbf{G}}_\tau - A_\tau \mathbf{G}_\tau - B_\tau \mathbf{U}_\tau\|_F^2,$$

of which the unique minimum-norm solution is given by

$$[A_\tau^\theta, B_\tau^\theta] = \bar{\mathbf{G}}_\tau \begin{bmatrix} \mathbf{G}_\tau \\ \mathbf{U}_\tau \end{bmatrix}^\dagger, \quad (27)$$

where $\mathbf{G}_\tau \in \mathbb{R}^{r \times \beta_\tau}, \bar{\mathbf{G}}_\tau \in \mathbb{R}^{r \times \beta_\tau}$ are defined in (14). Set

$$V_\tau = \bar{\mathbf{G}}_\tau \begin{bmatrix} \mathbf{G}_\tau \\ \mathbf{U}_\tau \end{bmatrix}^T, G_\tau = \begin{bmatrix} \mathbf{G}_\tau \\ \mathbf{U}_\tau \end{bmatrix} \begin{bmatrix} \mathbf{G}_\tau \\ \mathbf{U}_\tau \end{bmatrix}^T, M_\tau = [A_\tau^\theta, B_\tau^\theta],$$

then (27) is rewritten as $M_\tau = V_\tau G_\tau^{-1}$. As we obtain new state-control data pairs denoted by $\mathbf{X}_{\tau+1}, \bar{\mathbf{X}}_{\tau+1}$ and $\mathbf{U}_{\tau+1}$, matrices $V_{\tau+1}, G_{\tau+1}$ are updated by

$$V_{\tau+1} = [\bar{\mathbf{G}}_\tau \ \bar{\mathbf{G}}_{\tau+1}] \begin{bmatrix} \mathbf{G}_\tau & \mathbf{G}_{\tau+1} \\ \mathbf{U}_\tau & \mathbf{U}_{\tau+1} \end{bmatrix}^T = V_\tau + \bar{\mathbf{G}}_{\tau+1} \begin{bmatrix} \mathbf{G}_{\tau+1} \\ \mathbf{U}_{\tau+1} \end{bmatrix}^T,$$

and

$$G_{\tau+1} = \begin{bmatrix} \mathbf{G}_\tau & \mathbf{G}_{\tau+1} \\ \mathbf{U}_\tau & \mathbf{U}_{\tau+1} \end{bmatrix} \begin{bmatrix} \mathbf{G}_\tau & \mathbf{G}_{\tau+1} \\ \mathbf{U}_\tau & \mathbf{U}_{\tau+1} \end{bmatrix}^T = G_\tau + \begin{bmatrix} \mathbf{G}_{\tau+1} \\ \mathbf{U}_{\tau+1} \end{bmatrix} \begin{bmatrix} \mathbf{G}_{\tau+1} \\ \mathbf{U}_{\tau+1} \end{bmatrix}^T. \quad (28)$$

According to the Sherman–Morrison formula:

$$(A + uv^T)^{-1} = A^{-1} - \frac{A^{-1}uv^T A^{-1}}{\mathbf{I} + v^T A^{-1}u},$$

one has:

$$\begin{aligned}
M_{\tau+1} &= (V_\tau + \bar{\mathbf{G}}_{\tau+1} \chi_{\tau+1}^T) (G_\tau^{-1} - (G_\tau^{-1} \chi_{\tau+1} \chi_{\tau+1}^T G_\tau^{-1}) (\mathbf{I}_{\beta_{\tau+1}} + \chi_{\tau+1}^T G_\tau^{-1} \chi_{\tau+1}))^{-1} \\
&= M_\tau - \lambda_\tau M_\tau \chi_{\tau+1} \chi_{\tau+1}^T G_\tau^{-1} + \lambda_\tau \bar{\mathbf{G}}_{\tau+1} (\lambda_\tau^{-1} - \chi_{\tau+1}^T G_\tau^{-1} \chi_{\tau+1}) \chi_{\tau+1}^T G_\tau^{-1} \\
&= M_\tau - \lambda_\tau M_\tau \chi_{\tau+1} \chi_{\tau+1}^T G_\tau^{-1} + \lambda_\tau \bar{\mathbf{G}}_{\tau+1} \chi_{\tau+1}^T G_\tau^{-1} \\
&= M_\tau + (\bar{\mathbf{G}}_{\tau+1} - M_\tau \chi_{\tau+1}) \lambda_\tau \chi_{\tau+1}^T G_\tau^{-1},
\end{aligned}$$

where

$$\lambda_\tau = (\mathbf{I}_{\beta_{\tau+1}} + \chi_{\tau+1}^T G_\tau^{-1} \chi_{\tau+1})^{-1}, \chi_{\tau+1} = \begin{bmatrix} \mathbf{G}_{\tau+1} \\ \mathbf{U}_{\tau+1} \end{bmatrix},$$

and $C_{\tau+1}^\theta \in \mathbb{R}^{n \times r}$ is proved analogically. \blacksquare

Proof of Lemma 2. Consider a DNN with $h \geq 1$ hidden layers and recall that $\bar{\psi}^h = [\bar{\psi}_1^h, \bar{\psi}_2^h, \dots, \bar{\psi}_{n_h}^h]^T \in \mathbb{R}^{n_h}$ denotes its last hidden layer and $\bar{\psi}^o = [\bar{\psi}_1^o, \bar{\psi}_2^o, \dots, \bar{\psi}_r^o]^T \in \mathbb{R}^r$ denotes its output layer. Then $\bar{\psi}^o$ can be represented by $\bar{\psi}^h$ as

$$\bar{\psi}_i^o = \bar{\psi}_i^o \left(\sum_{j=1}^{n_h} \theta_{i,j}^h \bar{\psi}_j^h \right), \quad i = 1, 2, \dots, r,$$

where $\theta^h \in \mathbb{R}^{r \times n_h}$ denotes the weight matrix of the DNN's last hidden layer and $\bar{\psi}_i^o : \mathbb{R} \rightarrow \mathbb{R}, \bar{\psi}_j^h : \mathbb{R} \rightarrow \mathbb{R}$ are generally a nonlinear function chosen by the user.

Define $\phi = [\phi_1, \phi_2, \dots, \phi_r]^T \in \mathbb{R}^r$ with

$$\phi_i = \sum_{j=1}^{\infty} \theta_{i,j}^h \bar{\psi}_j^h, \quad i = 1, 2, \dots, r,$$

and $\|\phi\| = 1$. Let $\Phi = \begin{bmatrix} \phi \\ u \end{bmatrix}$ with $u \in \mathbb{R}^m$ denote the control input chosen from the control sequence \mathbf{u} . Recall the

projection operator from Definition 2. Let $P := \begin{bmatrix} P^{\mu_1} & \mathbf{0}_{n_h \times m} \\ \mathbf{0}_{m \times n_h} & P^{\mu_2} \end{bmatrix}$ with μ_1, μ_2 denoting the empirical measurements associated to the x_1, x_2, \dots, x_{n_h} and u_1, u_2, \dots, u_m , respectively. If Assumption 4 holds, according to Parseval's identity (i.e., $\sum_{i=1}^r \sum_{j=1}^{\infty} |\theta_{i,j}^h|^2 = 1$), one has

$$\begin{aligned}
\|P\Phi - \Phi\|^2 &= \left\| \begin{bmatrix} P^{\mu_1} \phi \\ P^{\mu_2} u \end{bmatrix} - \begin{bmatrix} \phi \\ u \end{bmatrix} \right\|^2 = \left\| \begin{bmatrix} \sum_{j=1}^{n_h} \theta_{1,j}^h \bar{\psi}_j^h - \sum_{j=1}^{\infty} \theta_{1,j}^h \bar{\psi}_j^h \\ \sum_{j=1}^{n_h} \theta_{2,j}^h \bar{\psi}_j^h - \sum_{j=1}^{\infty} \theta_{2,j}^h \bar{\psi}_j^h \\ \vdots \\ \sum_{j=1}^{n_h} \theta_{r,j}^h \bar{\psi}_j^h - \sum_{j=1}^{\infty} \theta_{r,j}^h \bar{\psi}_j^h \\ \mathbf{0}_m \end{bmatrix} \right\|^2 \\
&= \sum_{i=1}^r \sum_{j=n_h+1}^{\infty} |\theta_{i,j}^h|^2 \xrightarrow{n_h \rightarrow \infty} 0. \quad \blacksquare
\end{aligned}$$

Proof of Lemma 3. Recall the L_2 projection and \mathcal{F}_r from Definition 2. Before we start the proof, we introduce the following supporting lemma from [8].

Lemma 4 Let $\hat{\chi}_k = \begin{bmatrix} x_k \\ u_k \end{bmatrix}$ denote the state of the augmented system and μ_k be the empirical measurements with respect to the points $\hat{\chi}_1, \hat{\chi}_2, \dots, \hat{\chi}_k$ denoted by $\mu_k = \frac{1}{k} \sum_{i=1}^k \delta_{\hat{\chi}_i}$, where $\delta_{\hat{\chi}_i}$ denotes the Dirac measurement in $\hat{\chi}_i$. Then for any $f \in \mathcal{F}_r$,

$$K_D f = P_r^{\mu_k} \mathcal{K} f = \arg \min_{g \in \mathcal{F}_r} \|g - \mathcal{K} f\|_{L_2(\mu_k)}.$$

Remark 8 Lemma 4 shows that the approximated Koopman operator K_D is the L_2 projection of the Koopman operator \mathcal{K} in \mathcal{F}_r associated with the empirical measure supported in samples $\hat{\chi}_1, \hat{\chi}_2, \dots, \hat{\chi}_k$.

Then recall Φ, P defined in **Proof of Lemma 2** and rewrite Φ as $\Phi = P\Phi + (I - P)\Phi$. According to Lemma 4, one lets $K_D := PK$ be the approximated sequence of Koopman operators which leads to

$$\begin{aligned}
\|K_D P\Phi - \mathcal{K}\Phi\| &= \|PKP\Phi - \mathcal{K}\Phi\| = \|(P - I)\mathcal{K}P\Phi + \mathcal{K}(P - I)\Phi\| \\
&\leq \|(P - I)\mathcal{K}P\Phi\| + \|\mathcal{K}(P - I)\Phi\| \\
&\leq \|(P - I)\mathcal{K}\Phi\| + \|(P - I)(\mathcal{K}P - \mathcal{K})\Phi\| + \|\mathcal{K}\| \|(P - I)\Phi\|.
\end{aligned} \tag{29}$$

According to Lemma 2, one has

$$\lim_{n_h \rightarrow \infty} \|K_D P \Phi - \mathcal{K} \Phi\| = 0. \quad \blacksquare$$

Proof of Theorem 1. Abusing some notations, we first show that the estimation error in (20) is bounded. Recall that given the latest \mathcal{B}_τ with $\{x_{k-1}, u_{k-1}\}$ its latest data point (i.e., $x_{k-1} := x_{k_\tau + \beta_\tau}$, $u_{k-1} := u_{k_\tau + \beta_\tau}$), $x_k \in \mathbb{R}^n$ denotes the state of the system of the unknown NTVS evolving from $x_{k-1} \in \mathbb{R}^n$ and $u_{k-1} \in \mathbb{R}^m$. \hat{x}_k in (21) denotes the estimated state introduced by the proposed method. Here, we extend the estimation error in (20) as

$$\|e_k\| = \|x_k - \hat{x}_k + x_{k-1} - x_{k-1}\|. \quad (30)$$

For any $\bar{x} \in \mathcal{B}_\tau^x$, $\bar{u} \in \mathcal{B}_\tau^u$ (note that here $x_{k-1} = \bar{x}_{k-1}$, $u_{k-1} = \bar{u}_{k-1}$ since $\{x_{k-1}, u_{k-1}\}$ is the observed state-input data point), we introduce ϵ_k as the local estimation error induced by the system approximation in (10) given by

$$\epsilon_k = g(\bar{x}_k, \theta_\tau) - (A_\tau g(\bar{x}_{k-1}, \theta_\tau) + B_\tau \bar{u}_{k-1}).$$

Similarly, let $\bar{\epsilon}_k$ denote the approximation error induced by the minimization of (11) by

$$\bar{\epsilon}_k = \bar{x}_k - C_\tau g(\bar{x}_k, \theta_\tau),$$

which leads to

$$\bar{x}_{k-1} = C_\tau (A_\tau g(\bar{x}_{k-2}, \theta_\tau) + B_\tau \bar{u}_{k-2}) + C_\tau \epsilon_{k-1} + \bar{\epsilon}_{k-1}. \quad (31)$$

By substituting (21) and (31) into (30), we have the following.

$$\begin{aligned} \|e_k\| &= \|C_\tau A_\tau (g(\bar{x}_{k-2}, \theta_\tau) - g(\bar{x}_{k-1}, \theta_\tau)) + C_\tau B_\tau (\bar{u}_{k-2} - \bar{u}_{k-1}) + C_\tau \epsilon_{k-1} + x_k - \bar{x}_{k-1} + \bar{\epsilon}_{k-1}\|, \\ &\stackrel{(i)}{\leq} \|C_\tau A_\tau (g(\bar{x}_{k-2}, \theta_\tau) - g(\bar{x}_{k-1}, \theta_\tau))\| + \|C_\tau B_\tau (\bar{u}_{k-2} - \bar{u}_{k-1})\| + \|C_\tau \epsilon_{k-1}\| + \|x_k - \bar{x}_{k-1}\| \\ &\quad + \|\bar{\epsilon}_{k-1}\|, \\ &\stackrel{(ii)}{\leq} \|C_\tau A_\tau\| \|g(\bar{x}_{k-2}, \theta_\tau) - g(\bar{x}_{k-1}, \theta_\tau)\| + \|C_\tau B_\tau\| \|\bar{u}_{k-2} - \bar{u}_{k-1}\| + \|C_\tau\| \|\epsilon_{k-1}\| \\ &\quad + \|x_k - \bar{x}_{k-1}\| + \|\bar{\epsilon}_{k-1}\|, \end{aligned} \quad (32)$$

where (i) follows the triangle inequality and (ii) is derived by subordination and submultiplicativity.

For the first two terms of (32), if Assumptions 2-3 hold, one has

$$\|C_\tau A_\tau\| \|g(\bar{x}_{k-2}, \theta_\tau) - g(\bar{x}_{k-1}, \theta_\tau)\| \leq \|C_\tau A_\tau\| \mu_g \mu_x$$

and

$$\|C_\tau B_\tau\| \|\bar{u}_{k-2} - \bar{u}_{k-1}\| \leq \|C_\tau B_\tau\| \mu_u.$$

For writing convenience, one denotes

$$L_a := \|C_\tau A_\tau\| \mu_g \mu_x + \|C_\tau B_\tau\| \mu_u. \quad (33)$$

For the third term of (32), one can derive the error bound of $\|\epsilon_{k-1}\|$ by backpropagating it from k to $k_0 = 0$. Define the global approximation error in \mathcal{B}_τ as

$$\mathcal{E}_k = g(\bar{x}_k, \theta_\tau) - \prod_{i=0}^k A_i g(\bar{x}_0, \theta_0) - \sum_{j=0}^{k-1} \left(\prod_{l=0}^{k-j-1} A_l \right) B_j u_j. \quad (34)$$

The related proof is inspired by the global accumulation rule of ϵ_k of time-invariant systems proposed in [30] given by

$$E_k = \sum_{i=0}^{k-1} A^i \epsilon_{k-i}. \quad (35)$$

To achieve the error bound \mathcal{E}_k in (34), it is necessary to replace A in (35) with A_τ (note that the batch index τ is slower than the data point index k). Then \mathcal{E}_k is derived by induction, that is,

- when $\tau = 1$, $k \in [k_1, k_1 + \beta_1]$,

$$\mathcal{E}_k = \sum_{i=0}^{k-k_1-1} A_1^i \epsilon_{k-i} + A_1^{k-k_1-1} \sum_{j=1}^{\beta_0} A_0^j \epsilon_{k_1+1-j}, \quad (36)$$

- when $\tau > 1, k \in [k_\tau, k_\tau + \beta_\tau]$,

$$\mathcal{E}_k = \sum_{i=0}^{k-k_\tau-1} A_\tau^i \epsilon_{k-i} + A_\tau^{k-k_\tau-1} \left(\sum_{j=1}^{\beta_{\tau-1}} A_{\tau-1}^j \epsilon_{k_\tau+1-j} + \left(\sum_{l=1}^{\tau-1} \sum_{m=1}^{\beta_{l-1}} \left(\prod_{n=\tau-1}^l A_n^{\beta_n} \right) A_{l-1}^m \right) \epsilon_{k_l+1-m} \right), \quad (37)$$

- when $\tau + 1, k \in [k_{\tau+1}, k_{\tau+1} + \beta_{\tau+1}]$,

$$\mathcal{E}_k = \sum_{i=0}^{k-k_{\tau+1}-1} A_{\tau+1}^i \epsilon_{k-i} + A_{\tau+1}^{k-k_{\tau+1}-1} \left(\sum_{j=1}^{\beta_\tau} A_\tau^j \epsilon_{k_{\tau+1}+1-j} + \left(\sum_{l=1}^{\tau} \sum_{m=1}^{\beta_{l-1}} \left(\prod_{n=\tau}^l A_n^{\beta_n} \right) A_{l-1}^m \right) \epsilon_{k_l+1-m} \right). \quad (38)$$

According to (36)-(38), the third term of (32) is bounded by

$$\| C_\tau \epsilon_{k-1} \| \leq \| C_\tau \left(\sum_{i=0}^{k-k_\tau-2} A_\tau^i + A_\tau^{k-k_\tau-2} \left(\sum_{j=1}^{\beta_{\tau-1}} A_{\tau-1}^j + \sum_{l=1}^{\tau-1} \sum_{m=1}^{\beta_{l-1}} \left(\prod_{n=\tau-1}^l A_n^{\beta_n} \right) A_{l-1}^m \right) \right) \| L_1.$$

where

$$L_1 = \max_{\substack{\bar{x}_s \in \mathcal{B}_\tau^x \\ \bar{u}_s \in \mathcal{B}_\tau^u}} \| g(\bar{x}_{s+1}, \theta_\tau) - A_\tau g(\bar{x}_s, \theta_\tau) - B_\tau \bar{u}_s \| . \quad (39)$$

For the last two terms of (32), if Assumption 2 holds, one has

$$\| x_k - \bar{x}_{k-1} \| < \mu_x,$$

and since $\bar{\epsilon}_{k-1}$ is defined on \mathcal{B}_τ^x , one can compute its upper bound by

$$\| \bar{\epsilon}_{k-1} \| \leq L_2 = \max_{\bar{x} \in \mathcal{B}_\tau^x} \| \bar{x} - C_\tau g(\bar{x}, \theta_\tau) \| . \quad (40)$$

To sum up, recall L_1 in (39) and L_2 in (40), let

$$L_b := \| C_\tau \left(\sum_{i=0}^{k-k_\tau-2} A_\tau^i + A_\tau^{k-k_\tau-2} \left(\sum_{j=1}^{\beta_{\tau-1}} A_{\tau-1}^j + \sum_{l=1}^{\tau-1} \sum_{m=1}^{\beta_{l-1}} \left(\prod_{n=\tau-1}^l A_n^{\beta_n} \right) A_{l-1}^m \right) \right) \| L_1 \quad (41)$$

and

$$L_c := \mu_x + L_2, \quad (42)$$

the estimation error e_k in (30) is upper bounded by

$$\| e_k \| \leq L_a + L_b + L_c. \quad (43)$$

We further reduce the error bound derived in (43) based on Lemmas 2-3. Recall that $K_D := PK$ in (29) and let

$$\Phi_D^\tau(\bar{x}_k, \bar{u}_k) := [g(\bar{x}_k, \theta_\tau)^T, \bar{u}_k^T]^T.$$

According to Lemma 2 ($\lim_{n_h \rightarrow \infty} \Phi_D^\tau = \Phi^\tau$) and Lemma 3 ($\lim_{n_h \rightarrow \infty} K_D^\tau = \mathcal{K}^\tau$), by following the Definition of Koopman operator in 1, one has

$$\lim_{n_h \rightarrow \infty} K_D^\tau \Phi_D^\tau(\bar{x}_s, \bar{u}_s) = [\mathcal{K}^\tau \Phi^\tau](\bar{x}_s, \bar{u}_s) = \Phi^\tau(\bar{x}_{s+1}, \bar{u}_{s+1}). \quad (44)$$

Since we are interested in predicting the future values of the system state, we can only keep the first r rows of $\Phi_D^\tau(\bar{x}_{s+1}, \bar{u}_{s+1})$ and $K_D^\tau \Phi_D^\tau(\bar{x}_s, \bar{u}_s)$. Therefore, we define $\bar{\mathcal{K}}^\tau$ and \bar{K}_D^τ as the first r rows of \mathcal{K}^τ and K_D^τ , respectively, and decompose the matrix \bar{K}_D^τ as $\bar{K}_D^\tau =: [A_\tau, B_\tau]$. Then according to (44), one has

$$\lim_{n_h \rightarrow \infty} L_1 = \max_{\substack{\bar{x}_s \in \mathcal{B}_\tau^x \\ \bar{u}_s \in \mathcal{B}_\tau^u}} \| g(\bar{x}_{s+1}, \theta_\tau) - [\bar{\mathcal{K}}^\tau \Phi^\tau](\bar{x}_s, \bar{u}_s) \| = 0.$$

Finally, recall L_a in (33) and L_c in (42), one has

$$\lim_{n_h \rightarrow \infty} \sup \| e_k \| = (\| C_\tau A_\tau \| \mu_g + 1) \mu_x + \| C_\tau B_\tau \| \mu_u + \max_{\bar{x} \in \mathcal{B}_\tau^x} \| \bar{x} - C_\tau g(\bar{x}, \theta_\tau) \| . \quad \blacksquare$$

Proof of Corollary 1. Recall L_b in (41). If Assumption 5 holds, by following the properties of triangle inequality and submultiplicativity, one has $\| \sum_{i=0}^{\beta_\tau} A_\tau^i \| < \beta_\tau$ and $\| A_\tau^{\beta_\tau} \| < 1$, which leads to

$$L_b < \| C_\tau \| L_1(\beta_\tau + \beta_{\tau-1} + \| \sum_{l=1}^{\tau-1} \sum_{m=1}^{\beta_{l-1}} (\prod_{n=\tau-1}^l A_n^{\beta_n}) A_{l-1}^m \|).$$

Following the submultiplicativity, one has $\lim_{\tau \rightarrow \infty} \| \sum_{l=1}^{\tau-1} \sum_{m=1}^{\beta_{l-1}} (\prod_{n=\tau-1}^l A_n^{\beta_n}) A_{l-1}^m \| = \mu_c$ with μ_c a positive constant, which leads to

$$\lim_{\tau \rightarrow \infty} \sup L_b = \| C_\tau \| L_1(\beta_\tau + \beta_{\tau-1} + \mu_c). \quad (45)$$

By substituting (45) into (43), one can notice that $\lim_{k \rightarrow \infty} \sup \| e_k \|$ is determined by the minimization performance of (17) and μ_x, μ_u . ■